Local Conformational Transition of *Hydrogenobacter thermophilus* Cytochrome c_{552} Relevant to Its Redox Potential[†,‡]

Shin-ichi J. Takayama,[§] Yo-ta Takahashi,[§] Shin-ichi Mikami,[§] Kiyofumi Irie,[§] Shin Kawano,[§] Yasuhiko Yamamoto,*[,§] Hikaru Hemmi,[||] Ryo Kitahara,[⊥] Shigeyuki Yokoyama,[⊥,#,△] and Kazuyuki Akasaka[⊥,○]

Department of Chemistry, University of Tsukuba, Tsukuba 305-8571, Japan, National Food Research Institute, Tsukuba 305-8642, Japan, RIKEN SPring-8 Center, 1-1-1 Kouto, Sayo-cho, Sayo-gun, Hyogo 679-5148, Japan, RIKEN Genomic Sciences Center, 1-7-22 Suehiro-cho, Tsurumi, Yokohama 230-0045, Japan, Department of Biophysics and Biochemistry, Graduate School of Science, University of Tokyo, 7-3-1 Hongo, Bunkyo-ku, Tokyo 113-0033, Japan, and Department of Biotechnological Science, School of Biology-Oriented Science and Technology, Kinki University, 930 Nishimitani, Kinokawa, Wakayama 649-6493, Japan

Received January 15, 2007; Revised Manuscript Received June 7, 2007

ABSTRACT: In order to elucidate the molecular mechanisms responsible for the apparent nonlinear behavior of the temperature dependence of the redox potential of *Hydrogenobacter thermophilus* cytochrome c_{552} [Takahashi, Y., Sasaki, H., Takayama, S. J., Mikami, S., Kawano, S., Mita, H., Sambongi, Y., and Yamamoto, Y. (2006) *Biochemistry 45*, 11005−11011], its heme active site structure has been characterized using variable-temperature and -pressure NMR techniques. The study revealed a temperature-dependent conformational transition between protein structures, which slightly differ in the conformation of the loop bearing the Fe-bound axial Met residue. The heme environment in the protein structure which arises at lower temperature was found to be more polar, as a result of the altered orientation of the loop with respect to the heme due to its conformational change, than that arising at higher temperature. The present study demonstrated the importance of the structural and dynamic properties of the polypeptide chain in close proximity to the heme for redox regulation of the protein.

Proteins exhibit freedom of rotation, through their ϕ and ψ angles, that endows their polypeptide chains with intrinsic conformational flexibility. The three-dimensional structure of a native protein is determined by countless nonbonding molecular interactions, and hence the conformation of a native protein in nature is labile and crucially dependent upon the environment. As a consequence, a biologically active protein is a dynamic entity that can respond quickly to changes in its environment (*1*). This motility is often a key to protein function, and hence, in order to elucidate the functions of proteins, their static structures described by X-ray crystallographic coordinates must be augmented by the dynamic structures manifested in various spectroscopic data. Among a variety of spectroscopic techniques available for studies on protein dynamics, NMR is unique in terms of not only its sensitivity as to dynamic structures exhibiting a wide range of time scales but also its ability to provide information from which detailed descriptions of the dynamic structures of proteins in solution can be made.

Cytochrome *c* (cyt *c*),[1] in which the heme Fe is coordinated to a His and a Met as axial ligands at the redox center, is one of the best characterized redox proteins, and much has been learned about the overall properties that determine its redox activity (*2*). *Hydrogenobacter thermophilus* cyt c_{552} (HT) (*3*, *4*) and *Pseudomonas aeruginosa* cyt c_{551} (PA) (*5*) are composed of 80 and 82 amino acid residues, respectively, and exhibit high sequence identity (56%) (*3*) and hence almost identical protein folding (Figure 1) (*4*−*6*). Despite their structural similarity, HT and PA exhibit remarkably different redox properties (*7*). One of the major differences is the nonlinearity of plots of redox potentials (E_m) against temperature (E_m−T plots) for HT, as opposed to the usual linear E_m−T plots for PA (*7*) (Figure 2). Curvature was much more apparent in the plots of designed mutants (*8*). Similar nonlinear E_m−T plots have been reported for *Bacillus pasteurii* cyt c_{553} at pH 7.0 (*9*), bovine heart cyt *c* at pH 8.3 (*10*), and cyts c_2 (*11*) and cyts *c* (*12*) from various sources,

[†] This work was conducted as cooperative work under the JSPS Core to Core Program Action Initiative (no. 17009) and was also supported by a research grant (no. 17350081) from the Ministry of Education, Science, Sports, Culture, and Technology, the Yazaki Memorial Foundation for Science and Technology, the NOVARTIS Foundation (Japan) for the Promotion of Science, and the University of Tsukuba, Research Project (A).

[‡] The ^{15}N NMR assignments for PA and HT have been deposited in the Biological Magnetic Resonance Data Bank (BMRB) under entry numbers 10132 (oxidized PA), 10133 (reduced PA), 10134 (oxidized HT), and 10135 (reduced HT).

* Corresponding author. Phone/Fax: +81-29-853-6521. E-mail: yamamoto@chem.tsukuba.ac.jp.

[§] University of Tsukuba.

[||] National Food Research Institute.

[⊥] RIKEN SPring-8 Center.

[#] RIKEN Genomic Sciences Center.

[△] University of Tokyo.

[○] Kinki University.

[1] Abbreviations: cyt *c*, cytochrome *c*; PA, *Pseudomonas aeruginosa* cytochrome c_{551}; HT, *Hydrogenobacter thermophilus* cytochrome c_{552}; E_m, redox potential; E_m−T plots, plots of redox potentials of proteins against temperature; HSQC, heteronuclear single-quantum coherence; T_c, transition temperature, NE, *Nitrosomonas europaea* cytochrome c_{552}.

10.1021/bi7000714 CCC: $37.00
Published on Web 07/21/2007

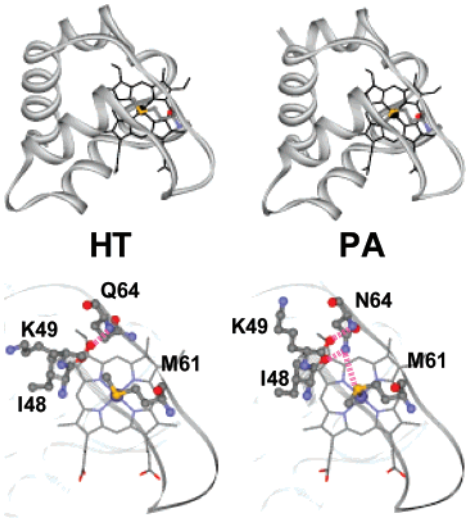

FIGURE 1: Schematic representation of *H. thermophilus* cytochrome c_{552} (HT) (PDB code 1YNR) (*4*) (left) and *P. aeruginosa* cytochrome c_{551} (PA) (PDB code 351C) (*5*) (right). The polypeptide chain is illustrated as a ribbon model and the heme as a wire model (top). The loop in close proximity to the heme, together with the amino acid residues at positions 48, 49, 61, and 64, is highlighted (bottom). The amino acid residues are illustrated as a ball and stick model. Pink broken lines indicate hydrogen bonds which are likely to contribute to the stability of the loop conformation, i.e., the K49−Q64 hydrogen bond in HT (*4*) and the I48−N64, K49−N64, and M61−N64 hydrogen bonds in PA (*5*).

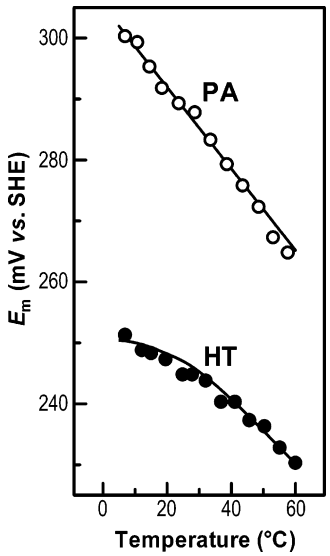

FIGURE 2: Plots of the redox potential (E_m) against temperature, E_m−T plots, for HT (filled circles) and PA (open circles) at pH 6.00 (*8*). The plots for HT exhibited an upward curvature, whereas those for PA could be fitted with a single straight line (see text).

which were attributed to a reversible conformational transition between low- and high-temperature forms (low-T and high-T forms, respectively) possessing distinctly different thermodynamic properties as to the redox reaction. Although the low-T and high-T forms of the proteins have been differentiated only by means of subtle changes in the heme environment (*9*−*13*), the structural factors responsible for the conformational transition between the low-T and high-T forms, and hence their distinctly different redox properties, have remained to be elucidated. Hence, detailed characterization of the conformational transition in HT is expected to provide valuable information about the molecular mechanisms responsible for the E_m control of the protein.

In the present study, we have characterized and compared the structural and dynamic properties of the heme active sites of HT and PA using variable-temperature and -pressure NMR. Since the freezing point of an aqueous solution decreases with increasing pressure, solution NMR well below 0 °C can be observed at an elevated pressure (*14*). Taking advantage of the high sensitivity of solution NMR as to protein structure, together with the use of low-temperature measurements down to −20 °C at 2000 bar, we could detect a conformational transition between protein structures for HT, which slightly differ in the conformation of the loop bearing the Fe-bound axial M61. The thermodynamic properties of the reduction of HT possessing different loop conformations suggested that the heme environment in the protein structure that arises at lower temperature is more polar, as a result of the altered orientation of the loop with respect to the heme due to its conformational change, than that arising at higher temperature. The conformational transition of a polypeptide chain in close proximity to the heme was found to be crucial for the E_m control of the protein.

MATERIALS AND METHODS

Protein Samples. The wild-type HT and PA were produced using *Escherichia coli* and purified as reported previously (*15*, *16*). Uniformly ^{15}N-labeled proteins were also prepared as described (*15*). The oxidized and reduced forms of the proteins were prepared by the addition of 10-fold molar excesses of potassium ferricyanide and sodium dithionite, respectively. For NMR samples, the proteins were concentrated to about 1 mM in an ultrafiltration cell (YM-5, Amicon), and then 10% ^2H_2O was added to the protein solutions. The pH of each sample was adjusted using 0.2 M KOH or 0.2 M HCl, and the pH was monitored with a Horiba F-22 pH meter with a Horiba type 6069-10C electrode.

Cyclic Voltammetry. Cyclic voltammograms of the proteins were obtained under a nitrogen atmosphere as described previously (*17*). A glassy carbon electrode (GCE) was polished with a 0.05 μm alumina slurry and then sonicated in deionized water for 1 min. Two microliters of a 1 mM protein solution was spread evenly with a microsyringe onto the surface of the GCE. Then the GCE surface was covered with a semipermeable membrane. All redox potentials (E_m) were referenced to a standard hydrogen electrode (SHE). The experimental error for E_m was ±5 mV. The variable temperature experiments were performed using a home-built nonisothermal electrochemical cell configuration, with which the temperature of the reference electrode was kept constant. The anodic to cathodic peak current ratios obtained at various potential scan rates (1−100 mV s^{-1}) were all ∼1. Both the anodic and cathodic peak currents increased linearly as a function of the square root of the scan rate in the range up to 100 mV s^{-1}. Thus, HT and PA, and their mutants exhibit quasi-reversible redox processes.

^{1}H NMR. NMR spectra were recorded on a Bruker DRX-800 or a Bruker Avance-600 FT NMR spectrometer operating at a ^{1}H frequency of 800 or 600 MHz, respectively. A pressure-resistant quartz cell with an active sample volume of ∼20 μL was used for the measurement of variable-

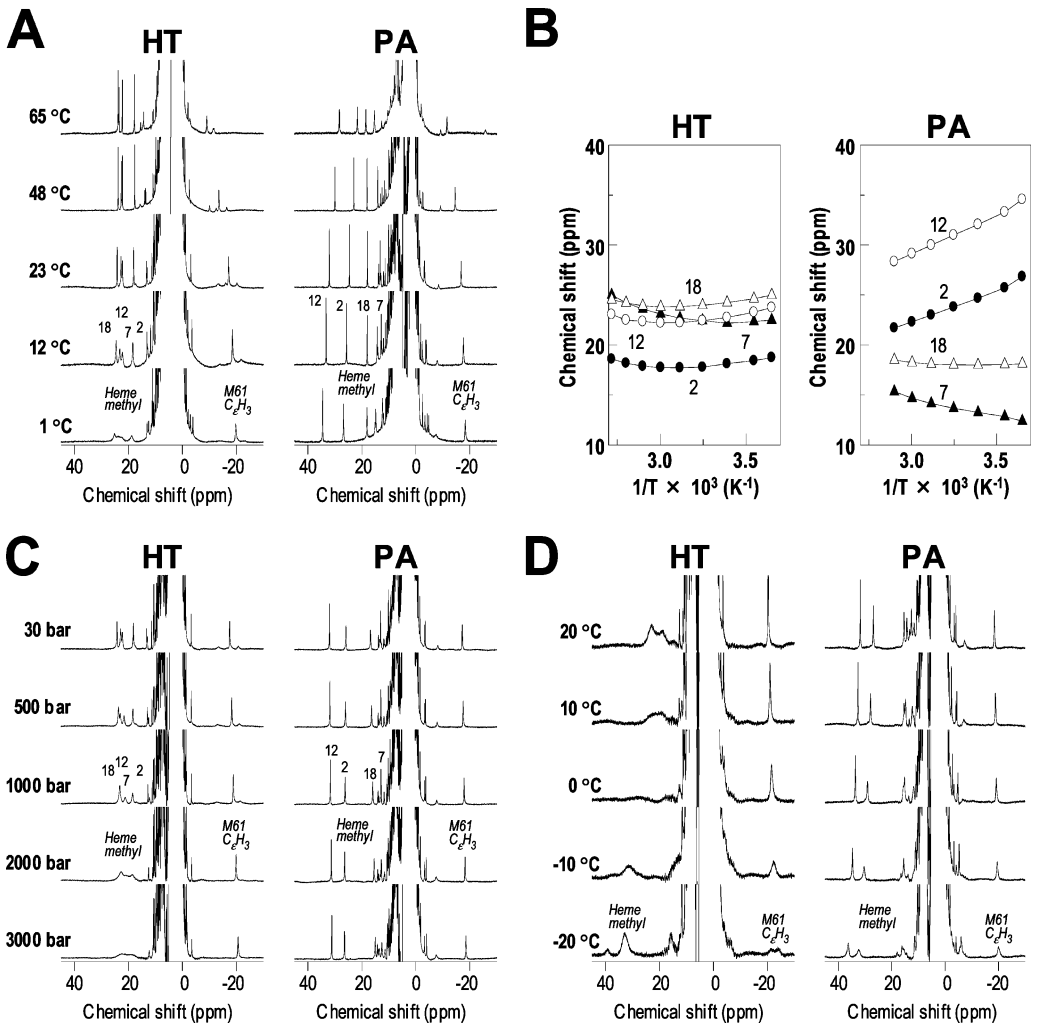

FIGURE 3: ^{1}H NMR spectra of oxidized HT and PA in 90% H_2O/10% D_2O, pH 7.00, at the indicated temperatures and ambient pressure (A), at pH 6.00, 25 °C, and the indicated pressures (C), and at pH 6.00, the indicated temperatures, and 2000 bar (D). Curie plots, i.e., paramagnetic shift vs reciprocal of absolute temperature, for heme methyl proton signals of the proteins at pH 7.00 and ambient pressure are shown in (B). The M61 $C_\gamma H$ proton signal of the oxidized PA observed at ~−40 ppm is not shown in the spectra. The assignments of heme methyl and M61 $C_\epsilon H_3$ proton signals (*27*, *55*) are given with the spectra. Heme proton signals of the oxidized HT exhibited line broadening at lower temperatures and higher pressures.

pressure NMR (*1*, *18*). The hydraulic pump used for controlling pressure was calibrated with a Heise gauge before use. The variable temperature control unit in the spectrometer was calibrated with standard temperature calibration samples of methanol and ethylene glycol. Sensitivity enhancement ^{15}N/^{1}H heteronuclear single-quantum coherence (HSQC) spectra were recorded using a standard pulse sequence. Spectra were zero-filled to give a final matrix of 2048 × 256 data points and apodized with a 90° shifted sine-bell window function in both dimensions. ^{1}H and ^{15}N chemical shifts were calibrated against the ^{1}H shift of sodium 2,2-dimethyl-2-silapentane-5-sulfonate (*19*).

RESULTS

^{1}H NMR Spectra of Oxidized HT and PA at Various Temperatures and Pressures. ^{1}H NMR spectra of oxidized HT at various temperatures and pressures are compared with those of oxidized PA in Figure 3. As was reported previously (*20*−*23*), with decreasing temperature from 65 to 1 °C, the line widths of the downfield-shifted heme proton signals of the oxidized HT broadened by ~600 Hz, while those of the corresponding signals of the oxidized PA did so only by ~50 Hz (Figure 3A). Interestingly, the heme methyl proton signals of the oxidized HT exhibited characteristic line broadening at lower temperatures such that the line widths of the heme 7- and 12-CH_3 proton signals were distinctly greater than those of the heme 2- and 18-CH_3 ones at lower temperatures; i.e., the line widths of the former and latter signals at 12 °C were ~350 and ~200 Hz, respectively, whereas those of all the heme methyl proton signals at 65 °C were ~50 Hz (Figure 3A). In addition, as has been reported for the oxidized forms of other cyts *c* (*24*, *25*), Curie plots, i.e., paramagnetic shift vs reciprocal of absolute temperature, of the paramagnetically shifted heme methyl proton signals of HT as well as PA did not obey the Curie law applicable to the systems of which the electronic and molecular structures are independent of temperature (Figure 3B), suggesting the possibility of a sizable contribution of excited states to their heme electronic structures in the ground state (*24*, *25*) and/or temperature-dependent structural changes in their heme active sites. Various low-spin Fe(III) model hemes and hemoproteins have been shown to be in thermal equilibrium between two states separated by an energy within several factors of thermal energy. The thermal equilibrium has been shown to

be manifested in anomalous temperature-dependent shifts of heme NMR signals. We have analyzed the temperature-dependent shifts of heme methyl proton signals of both oxidized HT and PA on the basis of an admixture of two energy states. Using the shifts of the reduced proteins (*6*, *15*) as the reference diamagnetic shifts for the corresponding proteins, the Curie plots for all of the heme methyl proton signals of the proteins were fitted to a reported equation (*26*) in order to estimate the energy gap (ΔE) between the ground and low-lying excited states (Supporting Information, SI 1). The ΔE values of ~20 and ~9 kJ mol^{-1} were obtained for HT and PA, respectively. Although the plots of HT could be fitted with the equation, the ΔE value of ~20 kJ mol^{-1} was well over the values reported for various low-spin Fe(III) model hemes and hemoproteins (*24*−*26*), and hence the anomalous temperature-dependent shifts of HT would not be due solely to the contribution of the excited state to its heme electronic structure in the ground state. This finding suggests the occurrence of temperature-dependent structural changes in the heme active site of HT, presumably the conformational transition between low-*T* and high-*T* forms (see below). In contrast, the ΔE value of ~9 kJ mol^{-1} obtained for PA was within the upper limit range of the values reported for model hemes and hemoproteins, indicating that the temperature-dependent structural change, if any, in its heme active site is small.

With increasing pressure from 30 to 3000 bar, the line widths of the heme proton signals of the oxidized HT broadened by more than 1000 Hz, while those of the corresponding signals of the oxidized PA did so only by ~10 Hz. On the other hand, the signals of both of the proteins exhibited shift changes of <1 ppm over the pressure range examined (Figure 3C). These results indicated that the activation volume of the conformational transition of HT is largely positive, as reflected in the broadening of the signals at higher pressure, and that the equilibrium of the transition, i.e., the population of low-*T* and high-*T* forms, was not so significantly affected by a pressure change. However, the pressure-induced shift changes of ~2 to ~3 ppm for the axial M61 $C_\epsilon H_3$ proton signals of the proteins suggested the occurrence of a structural alteration of the heme active site in the protein at higher pressure.

At an elevated pressure, the freezing temperature of water is depressed, and hence we could observe spectra in the temperature range down to −20 °C at 2000 bar. As shown in Figure 3D, the downfield-shifted heme proton signals of the oxidized HT broadened out almost completely at 0 °C and sharpened up with further decreasing temperature to −20 °C. Additionally, the signals exhibited progressive downfield shifts with decreasing temperature. Since observation of the axial M61 $C_\epsilon H_3$ proton signal at ~−22 ppm indicated that the Fe−Met coordination bond in the protein is intact under these conditions, the signals downfield-shifted to ~33 ppm in the spectrum of the oxidized HT at −20 °C can be attributed to the heme methyl protons of the protein structure which arises at lower temperatures. Hence these results suggested that the protein structures at ambient and lower temperatures, i.e., high-*T* and low-*T* forms, respectively, are in dynamic equilibrium. The difference in chemical shift between the signals of the high-*T* and low-*T* forms (i.e., the chemical shift difference of ~10 ppm between them corresponds to ~8000 Hz at a ^{1}H frequency of 800 MHz) yielded the value of ~10^4 s^{-1} as a transition rate under the conditions, 0 °C and 2000 bar, where the signals broadened out almost completely, i.e., the coalescence temperature and pressure (Figure 3D). Furthermore, with decreasing temperature from 20 to −20 °C at 2000 bar, the axial M61 $C_\epsilon H_3$ proton signal appeared to split into multiple components, with line broadening of ~1500 Hz. Therefore, the Met61 side chain of the low-*T* form would exhibit multiple conformational states under these conditions. In contrast to the case of HT, the line widths of the heme proton signals of the oxidized PA broadened only by ~50 and ~10 Hz over the temperature and pressure ranges of 1−65 °C and 30−3000 bar, respectively (panels A and C of Figure 3, respectively). But the broadening of the resolved signals of the oxidized PA at −20 °C and 2000 bar (Figure 3D) reflected a change in the heme active site structure in the protein under these conditions.

^{1}H NMR Spectra of Reduced HT at Various Temperatures. In order to clarify the paramagnetic contribution to the anomalous broadening of the HT signals, we next analyzed and compared the ^{1}H NMR spectra of reduced HT and PA at various temperatures. In the spectra of the reduced proteins (Figure 4), the W56 $N_\epsilon H$ and axial M61 $C_\epsilon H_3$ proton signals were resolved in the downfield- and upfield-shifted regions of the spectra, respectively (*6*, *27*). The line widths of the W56 $N_\epsilon H$ and M61 $C_\epsilon H_3$ proton signals of the reduced HT broadened by ~100 and ~20 Hz, respectively, over the temperature range of 1−78 °C, while those of the corresponding PA signals did so only by ~25 and ~5 Hz, respectively (Figure 4). The broadening of the signals of the reduced HT is likely to be related to the conformational transition responsible for the line broadening of the signals for the oxidized HT at lower temperatures. Thus the broadening of the HT signals at lower temperatures is independent of the magnetic property of heme iron.

^{15}N/^{1}H HSQC Spectra of the Oxidized and Reduced Forms of HT and PA at Various Temperatures and Pressures. We finally obtained ^{15}N/^{1}H HSQC spectra for both the oxidized and reduced forms of HT and PA at various temperatures and pressures in order to characterize the internal motion of the proteins (Figure 5 and Supporting Information, SI 2−SI 10). The cross-peaks exhibited distinct temperature- and pressure-induced shift changes in the ^{1}H and ^{15}N dimensions, which were totally reversible. The observed shift changes have been shown to reflect the protein structure primarily through the effects of temperature and pressure on the hydrogen bonds formed by the $N_\alpha H$ groups, as observed in other proteins (*28*−*34*). On the other hand, the line widths of the cross-peaks have been used as sensitive probes for detecting site-specific dynamic properties of protein structures (*28*, *30*). In the spectra of the reduced proteins, the cross-peaks of S53 and Q64 of HT exhibited much greater broadening at lower temperatures than those of the corresponding residues of PA, i.e., Q53 and N64 (Figure 5 and Supporting Information, SI 6 and SI 7). Thus distinct differences in the dynamic properties between the two proteins were clearly manifested in the temperature dependence of the line widths of these cross-peaks. As shown in Figure 6, the residues of which the HSQC cross-peaks exhibited broadening at lower temperatures were mostly found in the loop region bearing the axial M61 in HT, demonstrating the occurrence of a conformational change in this loop.

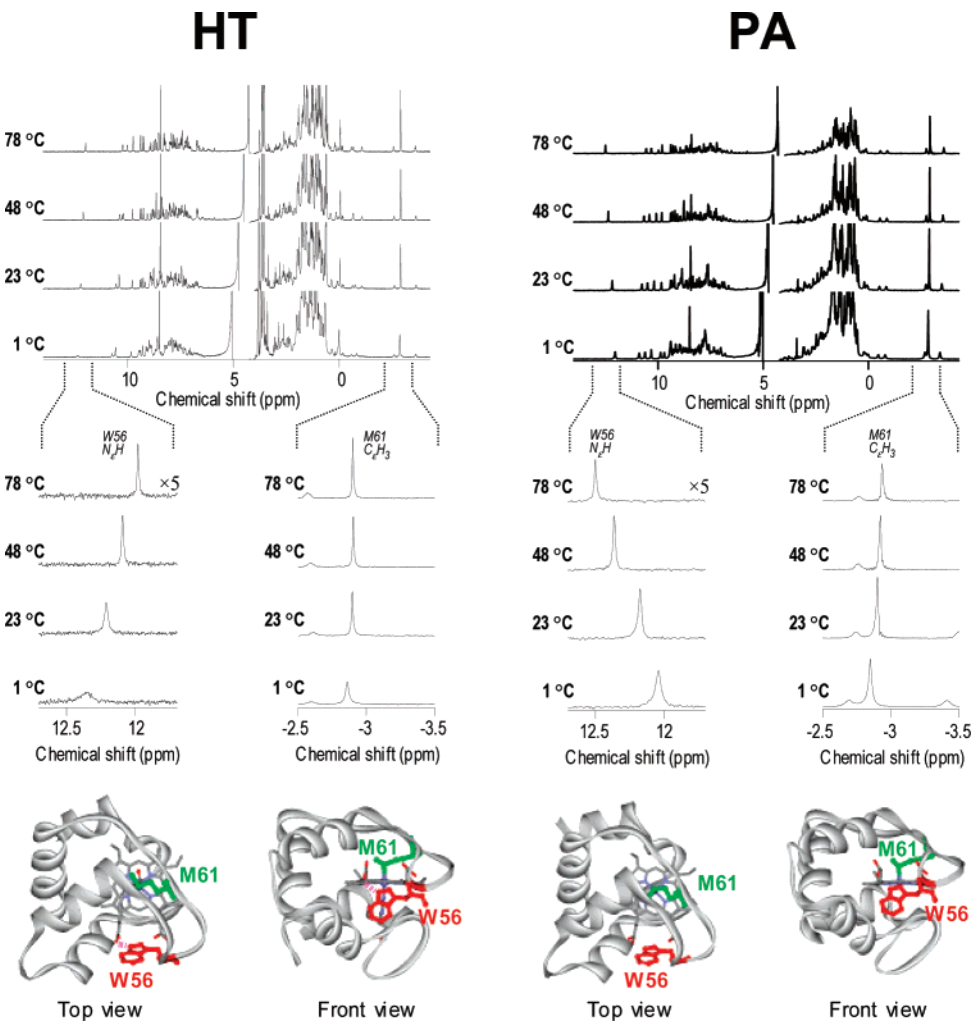

FIGURE 4: ^{1}H NMR spectra of reduced HT (left) and PA (right) in 90% H_2O/10% D_2O, pH 7.00, at the indicated temperatures (top), expansion of the W56 $N_\epsilon H$ and axial M61 $C_\epsilon H_3$ proton signals (middle), and locations of W56 and M61 in HT (PDB code 1YNR) and PA (PDB code 451C) (*4*) (bottom). The W56 $N_\epsilon H$ and axial M61 $C_\epsilon H_3$ proton signals of HT exhibited line broadening at lower temperatures.

DISCUSSION

Temperature-Dependent Conformational Transition in HT. The paramagnetically shifted heme peripheral side chain proton signals of hemoproteins have been shown to be highly sensitive to the structural features of their heme active sites (*35*−*37*). As reported previously (*20*−*23*), anomalous line broadening occurred selectively for the paramagnetically shifted heme proton signals of oxidized HT at lower temperatures (Figure 3A). Zhong et al. (*20*) have demonstrated that the line broadening of the signals of oxidized HT at lower temperatures is due to time-dependent modulation of the heme electronic structure through a conformational change of the protein, because the spin−lattice relaxation times of these protons were essentially independent of temperature; i.e., the relaxation times were ∼120 to ∼190 ms over the temperature range of 284−344 K (*20*). In the present study, the heme proton signals arising from the low-*T* form have been identified in the spectra obtained below −10 °C at 2000 bar (Figure 3D). The conformational changes of the axial H16 and M61 side chains, relative to the heme, could be potential candidates for the time-dependent modulation of the heme electronic structure responsible for the anomalous line broadening of the heme proton signals of oxidized HT. However, considering the limited freedom of the axial H16 side chain conformation in cyt *c* (*38*) as well as the conserved H16 coordination structure in both HT and PA (*4*, *5*, *38*), it is unlikely that the axial H16 coordination structure in HT is significantly affected by temperature changes, unless the protein unfolds. On the other hand, relatively large freedom is possible for the axial M61 side chain conformation (Figure 1). In fact, the line width of the M61 $C_\epsilon H_3$ proton signal of the reduced HT broadened by ∼20 Hz over the temperature range of 1−78 °C (Figure 4), demonstrating the occurrence of a conformational change of the axial M61 side chain. Furthermore, analysis of the ^{15}N/^{1}H HSQC cross-peaks observed at various temperatures revealed the occurrence of a conformational change of the loop bearing the axial M61 at lower temperatures (Figure 6). The conformational change of not only the axial Met61 side chain but also the loop is consistent with a large positive activation volume associated with the conformational transition between the low-*T* and high-*T* forms (Figure 3C). This conformational transition is likely to be responsible for the nonlinear E_m−T plots of HT (Figure 2).

The conformational change of the loop results in alteration of the axial M61 coordination structure, which in turn modulates the heme electronic structure through the interaction of the lone pair of the S_δ atom with the d_π (d_{xz} and d_{yz})

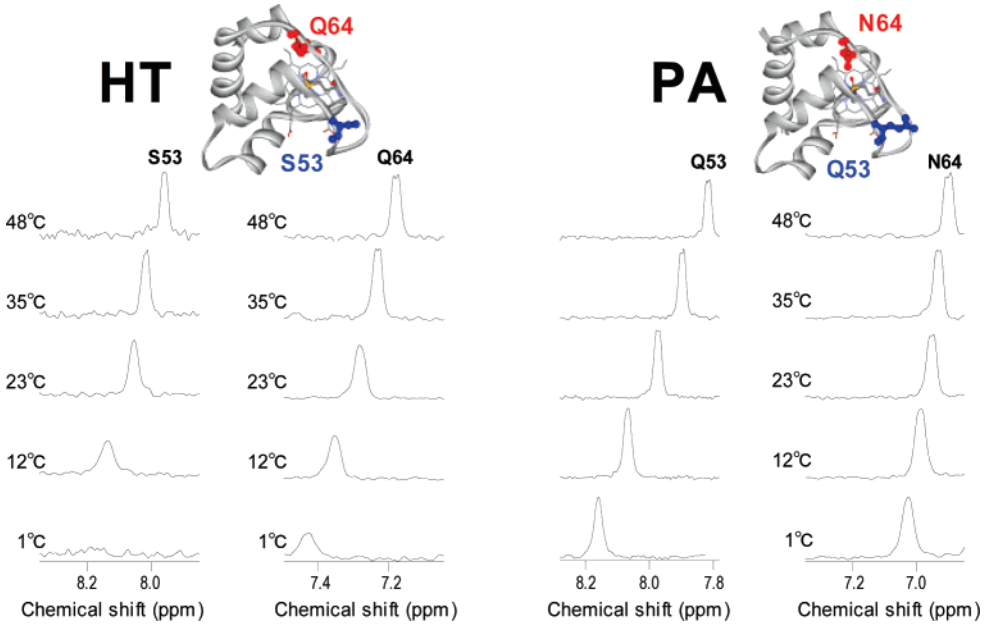

FIGURE 5: $^{15}N/^{1}H$ HSQC slices, along the ^{1}H axis, of $N_{\alpha}H$ cross-peaks of S53, Q64 and Q53, N64 of the reduced forms of ^{15}N uniformly labeled HT (left) and PA (right), respectively, in 90% H_2O/10% D_2O, pH 6.00, at the indicated temperatures. The locations of the amino acid residues at positions 53 and 64 in HT (PDB code 1YNR) (*4*) and PA (PDB code 351C) (*5*) are illustrated in the inset. The line widths of the HT cross-peaks were greater than those of the PA cross-peaks at lower temperatures.

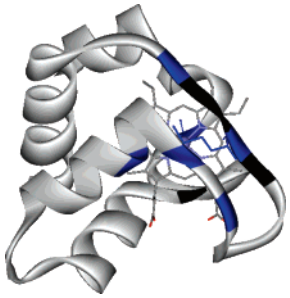

FIGURE 6: The residues in the reduced HT, of which the amide $N_{\alpha}H$ HSQC cross-peaks exhibited broadening at lower temperatures, i.e., H16, K47, G51, S53, M61, and Q64, are indicated in blue. Pro residues which give no cross-peak are indicated in black.

orbitals of heme Fe (*39*−*44*). The paramagnetically shifted heme proton signals of the protein are highly sensitive to the coordination structures of the axial ligands, as manifested in the large difference in the shift pattern of the heme methyl proton signals between the oxidized HT and PA (Figure 3A). Since the M61 side chain in HT is rather extended with a χ_2 angle of 177° (*4*), as opposed to the value of 166° for PA (*5*), the conformation of the M61 side chain in HT would be more directly and sensitively affected by a change in the loop conformation than that in PA. The rotation around the M61 S_{δ}−Fe bond as well as the changes in both the M61 S_{δ}−Fe bond length and tilt, relative to heme normal, contributes to the modulation of the heme electronic structure (*45*). Thus, the line broadening of the heme proton signals of HT at lower temperatures could be explained in terms of the alteration in the M61 coordination structure, which is accompanied with the conformational change of the loop. On the other hand, in contrast to the heme proton signals, the axial M61 $C_{\epsilon}H_3$ proton signal of HT was not so significantly affected by the alteration in the Met61 coordination structure (Figure 3A). Judging from the remarkable similarity in the Met61 $C_{\epsilon}H_3$ proton shift between the oxidized HT and PA (Figure 3A), the signal at ambient temperature appeared to be insensitive in nature to the Met61 coordination structure; i.e., the M61 $C_{\epsilon}H_3$ proton shifts of the oxidized HT and PA are −17.1 and −16.8 ppm at 23 °C, respectively.

The effect of the conformational change of the loop on the heme environment was manifested in the differential line broadening of the heme methyl proton signals of the oxidized HT at lower temperatures. Among the four heme methyl groups in HT, the 7- and 12-CH_3 groups are barely covered by the loop and hence are more exposed to the solvent than the 2- and 18-CH_3 ones, which are buried in the protein interior (Figure 1). Hence the chemical environment of the heme 7- and 12-CH_3 groups is more sensitive to a conformational change of the loop than that of the 2- and 18-CH_3 ones. Since paramagnetic shifts of heme proton signals have been shown to be influenced by the heme environment (*46*), the shifts of the heme 7- and 12-CH_3 proton signals of the oxidized HT are affected by both the change in the chemical environment, due to the altered orientation of the loop with respect to the heme, and the modulation of the heme electronic structure, induced by the change in the M61 coordination structure through the conformational change of the loop. Thus, the chemical shifts of the heme 7- and 12-CH_3 proton signals are expected to be more greatly influenced by the conformational equilibrium between the low-*T* and high-*T* forms of the protein than those of the heme 2- and 18-CH_3 ones. As a result, the line widths of the heme 7- and 12-CH_3 proton signals were distinctly larger than those of the heme 2- and 18-CH_3 ones at lower temperatures. The dielectric constant of bulk water increases with decreasing temperature, and hence a temperature-dependent conformational transition of the loop in HT would be induced through a polarity change of the environment, because a loop region generally possesses a large solvent-accessible surface area and excluded volume. The heme Fe coordination structure in HT at lower temperatures could be in principle inferred from the results of analysis of the paramagnetic shifts of the

heme proton signals (*45*). However, such a study is hampered at present by the difficulty in the assignment of the signals of the oxidized HT at lower temperatures.

The present variable-temperature and -pressure NMR studies indicated that the broadening of the oxidized HT signals at lower temperatures is due to a conformational transition of the loop region bearing the Met residue, which occurs in both the reduced and oxidized proteins. On the other hand, Zhong et al. (*20*) had attributed the line broadening of the heme methyl proton signals of the oxidized HT at lower temperatures to the chemical exchange, in which the Fe-bound M61 S_δ atom inverts between two different configurations. According to the proposal of Zhong et al. (*20*), the chemical exchange occurs at any temperature, and hence the heme methyl proton shift pattern of the protein reflects the average rate of fast exchange between two states with different paramagnetic shift patterns due to flipping of the chirality of the M61 S_δ atom. On the basis of this proposal, an exchange rate of $\sim 10^5$ s^{-1} has been estimated from a simulation of the heme methyl proton paramagnetic shift pattern (*20*). It is not obvious from our results whether inversion of the M61 S_δ atom configuration occurs in HT as well as whether the conformational transition of the loop bearing the Met residue in the protein is associated with flipping of the chirality of the M61 S_δ atom. The similarity between the rates estimated for the conformational transition of the loop region bearing the Met residue and the flipping of the chirality of the M61 S_δ atom, i.e., $\sim 10^4$ and $\sim 10^5$ s^{-1} for the former at 0 °C and 2000 bar and the latter at ambient temperature and pressure, respectively, is most likely to be just a coincidence. Furthermore, as far as functional consequences of the dynamic nature of the heme active site structure of the protein are concerned, the nonlinear E_m-T plots could not be accounted for by the flipping of the chirality of the iron-bound Met side chain, which has been proposed to occur throughout the accessible temperature range (*20*).

The present study demonstrated that the loop region bearing the axial M61 in HT yields a high-*T* form, possibly described by X-ray crystallographic coordinates (*4*), at ambient temperature, and with decreasing temperature, a low-*T* form arises. The high-*T* and low-*T* forms exchange faster than the NMR time scale, and the latter dominates at −20 °C at 2000 bar. The occurrence of a conformational change around the heme of HT was also supported by the results of analysis of the temperature-dependent shifts of the heme methyl proton signals, which suggested the presence of temperature-dependent structural changes in its heme active site, in addition to the contribution of low-lying excited states to its heme electronic structures in the ground state (*24*−*26*). The curvature of the E_m-T plots could be reasonably explained in terms of the temperature-dependent structure changes of the protein revealed in the present study.

Loop Structures of HT and PA. The loops bearing the axial M61 in HT and PA consist of 15 amino acid residues, i.e., the residues at positions 52−66, the homology being 60% (see Supporting Information, SI 11) (*4*, *5*). Most of the residues in the loop are involved in intramolecular hydrogen bond networks (see Supporting Information, SI 12), and these hydrogen bonds, together with the presence of three Pro residues, reduce the conformational freedom of the loop in HT. The hydrogen bond networks in the loop of PA are similar to those of HT, the exception being the formation of a unique tetrad hydrogen bond network, i.e., the N64 $N_\alpha H$, $N_\delta H$, and $N_{\delta'} H$ protons are hydrogen-bonded to K49 CO, I48 CO, and M61 S_δ, respectively, and the presence of an additional Pro residue (*5*) (see Supporting Information, SI 12). The importance of the residue at position 64 in the anomalous line broadening of the signals of HT at lower temperatures has been demonstrated through studies on a series of designed mutants (*8*, *22*, *23*). The M61−N64 hydrogen bond in the tetrad hydrogen bond network has been proposed to suppress the conformational change of the axial M61 side chain in PA (*22*). However, the observation of similar line broadening of heme proton signals of the oxidized form of *Nitrosomonas europaea* cyt c_{552} (NE) at low temperatures argued against this proposal, because the M61−N64 hydrogen bond appeared to be conserved in NE (*47*). NE is homologous to both HT and PA and hence possesses a loop bearing axial M61, of which the structural properties are similar to those of the other two proteins. NE possesses N64 as PA does, and the orientation of the N64 side chain, relative to the heme, in NE was thought to be similar to that in PA, because the ^{1}H NMR shift pattern of the N64 proton signals of reduced NE is remarkably similar to that of reduced PA; i.e., the N64 $N_\alpha H$, $C_\alpha H$, $C_\beta H$, $C_{\beta'} H$, $N_\delta H$, and $N_{\delta'} H$ proton shifts are 6.48, 4.71, 2.29, 2.39, 7.11, and 3.35 ppm for the former at pH 7 and 323 K, respectively (*47*), and 6.89, 4.80, 2.05, 2.43, 7.23, and 3.19 ppm for the latter at pH 5.2 and 323 K, respectively (*27*). The unusual upfield shifts of the $N_{\delta'} H$ proton signals of both proteins, due to the porphyrin ring current of the heme, indicated that the N64 $N_{\delta'} H$ proton is hydrogen-bonded to the Fe-bound M61 S_δ atom, located ∼0.24 nm away from the heme Fe, in the protein.

The unique tetrad K49−N64−I48/M61 hydrogen bond network in PA appears to contribute significantly to the stability of the loop conformation (*5*). According to the solution NMR structure of the reduced NE (*47*), I48 CO is not hydrogen-bonded to the N64 $N_{\delta'} H$ proton, but to both the G50 and G51 $N_\alpha H$ protons, and hence the K49−N64−I48/M61 tetrad hydrogen bond network is not formed in NE. The K49−N64 and N64−I48 hydrogen bonds in the tetrad K49−N64−I48/M61 network, which links the ends of the loop, appear to play important roles in stabilizing the overall loop conformation in the proteins, and hence, due to the lack of these hydrogen bonds, the loop by NE would be more susceptible to a conformational change than that in PA. In fact, as manifested in the line broadening of the HSQC cross-peak of Q64 of the reduced HT at lower temperatures (Figure 5), the K49−Q64 hydrogen bond alone was not strong enough to suppress the conformational change of the loop in the protein at lower temperatures. Furthermore, Chen et al. (*48*) found in NMR studies on PA, NE, and homologous proteins that the heme active site structures of the proteins adapt multiple conformational states, when the axial Met61 is displaced by exogenous ligands such as CN^- and OH^-, and that some conformational states are in dynamic exchange. Therefore, the heme active site structure of the protein appeared to be determined and stabilized by the formation of the axial coordination bonds and intramolecular hydrogen bond network, together with various nonbonding interactions.

Functional Consequences of the Conformational Transition. We finally discuss the functional consequences of the

conformational transition of the loop in HT. The E_m-T plots of HT exhibited upward curvature. We have shown that the nonlinearity of the E_m-T plots correlates well with the occurrence of line broadening of the heme proton signals at lower temperatures (*7*, *8*). Considering the NMR results, which indicated that the conformational equilibrium between the low-*T* and high-*T* forms of the protein occurs in a rather wide temperature range, thermodynamic parameters, i.e., ΔH and ΔS, for the redox reaction of the low-*T* form could not be determined from the plots shown in Figure 2. Nevertheless, the upward curvature of the E_m-T plots reflected that the ΔH and ΔS values of the low-*T* form are both less negative than the corresponding values of the high-*T* one.

The less negative ΔH value of the low-*T* form, compared with that of the high-*T* one, can be attributed to either stabilization of the oxidized protein and/or destabilization of the reduced one in the low-*T* form (*49*, *50*). The heme environment is crucial for the stability of the protein, and the increased polarity of the heme environment in the low-*T* form accounts for both the stabilization and destabilization of the oxidized and reduced proteins, respectively (see below). The polarity of the heme environment in the protein is related to the degree of exposure of the heme to the solvent, which is likely to be predominantly determined by the orientation of the loop relative to the heme in the protein (Figure 1). As described above, a temperature-dependent conformational transition occurs in the loop of HT.

With the more polar heme environment in the low-*T* form than the high-*T* one, the cationic ferriheme in the oxidized protein is more stabilized, and in contrast, the neutral ferroheme in the reduced one is more destabilized, resulting in the less negative ΔH value of the low-*T* form. On the other hand, the negative ΔS value for cyt *c* has been attributed to solvent ordering (*51*) and the decrease of the polarity of the heme environment upon reduction (*52*). The oxidized protein with a more polar heme environment is expected to possess more ordered solvent molecules because of the presence of the cationic ferriheme, whereas the effect of the polarity change of the heme environment in the reduced protein on solvent ordering could be rather small due to its neutral ferroheme. Consequently, in the framework for native folding, the ΔS value for the protein becomes less negative with increasing polarity of the heme environment. Thus, the difference in the E_m value between the low- and high-*T* forms of HT could be explained by the proposed conformational change of the loop. The functional relevance of the ligand-containing loop has been demonstrated for other metalloproteins (*53*, *54*).

CONCLUDING REMARKS

In order to elucidate the differences in functional properties between homologous HT and PA, their protein dynamics and conformation have been characterized and compared using variable-temperature and -pressure NMR. Despite their structural similarity, the study revealed a remarkable difference in the dynamic properties of the loop in close proximity to the heme between them. The loop of HT was found to be involved in the conformational transition at lower temperature, which resulted in nonlinear E_m-T plots. In contrast to HT, the loop of PA is not involved in the conformational transition. Scrutiny of the architecture of their protein structures suggested that the suppression of the conformational transition in PA is presumably due to the formation of a unique hydrogen bond network among four amino acid residues.

ACKNOWLEDGMENT

We thank Drs. Hajime Mita (Fukuoka Institute of Technology), Yoshihiro Sambongi (Hiroshima University), and Jun Hasegawa (Daiichi Sankyo Co., Ltd.) for useful comments. The ^{1}H NMR spectra were recorded on a Bruker AVANCE-600 spectrometer at the Chemical Analysis Center, University of Tsukuba.

SUPPORTING INFORMATION AVAILABLE

Analysis of Curie plots of the heme methyl proton shifts of oxidized HT and PA, superpositioning of ^{15}N/^{1}H HSQC spectra of the oxidized forms of ^{15}N uniformly labeled HT and PA in 90% H_2O/10% D_2O, pH 6.00, at various temperatures from 1 to 48 °C, and at 0 °C and various pressures from 30 to 3000 bar, superpositioning of ^{15}N/^{1}H HSQC spectra of the reduced forms of ^{15}N uniformly labeled HT and PA in 90% H_2O/10% D_2O, pH 6.00, at various temperatures from 1 to 48 °C, ^{15}N/^{1}H HSQC slices, along the ^{1}H axis, of N_αH cross-peaks of the amino acid residues at positions 15, 24, and 64 in the oxidized forms of ^{15}N uniformly labeled HT and PA in 90% H_2O/10% D_2O, pH 6.00, at various temperatures, a summary of the hydrogen bond networks in HT [PDB code 1YNR (*4*)] and PA [PDB code 351C (*5*)], and schematic representations of the hydrogen bond networks in the loops of HT and PA. This material is available free of charge via the Internet at http://pubs.acs.org.

REFERENCES

1. Akasaka, K. (2006) Probing conformational fluctuation of proteins by pressure perturbation, *Chem. Rev. 106*, 1814−1835.
2. Moore, G. R., and Pettigrew, G. W. (1990) *Cytochromes c: Evolutionary, Structural, and Physicochemical Aspects*, Springer-Verlag, Berlin.
3. Sanbongi, Y., Ishii, M., Igarashi, Y., and Kodama, T. (1989) Amino acid sequence of cytochrome c-552 from a thermophilic hydrogen-oxidizing bacterium, *Hydrogenobacter thermophilus*, *J. Bacteriol. 171*, 65−69.
4. Travaglini-Allocatelli, C., Gianni, S., Dubey, V. K., Borgia, A., Di Matteo, A., Bonivento, D., Cutruzzola, F., Bren, K. L., and Brunori, M. (2005) An obligatory intermediate in the folding pathway of cytochrome c_{552} from *Hydrogenobacter thermophilus*, *J. Biol. Chem. 280*, 25729−25734.
5. Matsuura, Y., Takano, T., and Dickerson, R. E. (1982) Structure of cytochrome c_{551} from *Pseudomonas aeruginosa* refined at 1.6 Å resolution and comparison of the two redox forms, *J. Mol. Biol. 156*, 389−409.
6. Hasegawa, J., Yoshida, T., Yamazaki, T., Sambongi, Y., Yu, Y., Igarashi, Y., Kodama, T., Yamazaki, K., Kyogoku, Y., and Kobayashi, Y. (1998) Solution structure of thermostable cytochrome *c*-552 from *Hydrogenobacter thermophilus* determined by ^{1}H-NMR spectroscopy, *Biochemistry 37*, 9641−9649.
7. Takahashi, Y., Sasaki, H., Takayama, S. J., Mikami, S., Kawano, S., Mita, H., Sambongi, Y., and Yamamoto, Y. (2006) Further enhancement of the thermostability of *Hydrogenobacter thermophilus* cytochrome c_{552}, *Biochemistry 45*, 11005−11011.
8. Takahashi, Y., Takayama, S. J., Mikami, S., Mita, H., Sambongi, Y., and Yamamoto, Y. (2006) Influence of a single amide group on the redox function of *Pseudomonas aeruginosa* cytochrome c_{551}, *Chem. Lett. 35*, 528−529.
9. Benini, S., Borsari, M., Ciurli, S., Dikiy, A., and Lamborghini, M. (1998) Modulation of *Bacillus pasteurii* cytochrome c_{553}

reduction potential by structural and solution parameters, *J. Biol. Inorg. Chem. 3*, 371−382.
10. Ikeshoji, T., Taniguchi, I., and Hawkridge, F. W. (1989) Electrochemically distinguishable states of ferricytochrome *c* and their transition with changes in temperature and pH, *J. Electroanal. Chem. 270*, 297−308.
11. Battistuzzi, G., Borsari, M., Sola, M., and Francia, F. (1997) Redox thermodynamics of the native and alkaline forms of eukaryotic and bacterial class I cytochromes *c*, *Biochemistry 36*, 16247−16258.
12. Battistuzzi, G., Borsari, M., Cowan, J. A., Eicken, C., Loschi, L., and Sola, M. (1999) Redox chemistry and acid-base equilibria of mitochondrial plant cytochromes *c*, *Biochemistry 38*, 5553−5562.
13. Battistuzzi, G., Borsari, M., and Sola, M. (2001) Medium and temperature effects on the redox chemistry of cytochrome *c*, *Eur. J. Inorg. Chem. 2001*, 2989−3004.
14. Eisenberg, D., and Kauzmann, W. (1969) *The Structure and Properties of Water*, Oxford at Clarendon Press, London.
15. Hasegawa, J., Shimahara, H., Mizutani, M., Uchiyama, S., Arai, H., Ishii, M., Kobayashi, Y., Ferguson, S. J., Sambongi, Y., and Igarashi, Y. (1999) Stabilization of *Pseudomonas aeruginosa* cytochrome c_{551} by systematic amino acid substitutions based on the structure of thermophilic *Hydrogenobacter thermophilus* cytochrome c_{552}, *J. Biol. Chem. 274*, 37533−37537.
16. Oikawa, K., Nakamura, S., Sonoyama, T., Ohshima, A., Kobayashi, Y., Takayama, S. J., Yamamoto, Y., Uchiyama, S., Hasegawa, J., and Sambongi, Y. (2005) Five amino acid residues responsible for the high stability of *Hydrogenobacter thermophilus* cytochrome c_{552}, *J. Biol. Chem. 280*, 5527−5532.
17. Lojou, E., and Bianco, P. (2000) Membrane electrodes can modulate the electrochemical response of redox Proteins−Direct electrochemistry of cytochrome *c*, *J. Electroanal. Chem. 485*, 71−80.
18. Akasaka, K., and Yamada, H. (2001) On-line cell high pressure nuclear magnetic resonance technique: application to protein studies, *Methods Enzymol. 338*, 134−158.
19. Wishart, D. S., Bigam, C. G., Yao, J., Abildgaard, F., Dyson, H. J., Oldfield, E., Markley, J. L., and Sykes, B. D. (1995) ^{1}H, ^{13}C and ^{15}N chemical shift referencing in biomolecular NMR, *J. Biomol. NMR 6*, 135−140.
20. Zhong, L., Wen, X., Rabinowitz, T. M., Russell, B. S., Karan, E. F., and Bren, K. L. (2004) Heme axial methionine fluxionality in *Hydrogenobacter thermophilus* cytochrome c_{552}, *Proc. Natl. Acad. Sci. U.S.A. 101*, 8637−8642.
21. Bren, K. L., Kellog, J. A., Kaur, R., and Wen, X. (2004) Folding, conformational changes, and dynamics of cytochrome *c* probed by NMR spectroscopy, *Inorg. Chem. 43*, 2934−2944.
22. Wen, X., and Bren, K. L. (2005) Suppression of axial methionine fluxion in *Hydrogenobacter thermophilus* Gln64Asn cytochrome c_{552}, *Biochemistry 44*, 5225−5233.
23. Wen, X., and Bren, K. L. (2005) Heme axial methionine fluxion in *Pseudomonas aeruginosa* Asn64Gln cytochrome c_{551}, *Inorg. Chem. 44*, 8587−8593.
24. Shokhirev, N. V., and Walker, F. A. (1995) Analysis of the temperature dependence of the ^{1}H contact shifts of β-pyrrole substituents in low-spin Fe(III) model hemes and heme proteins: explanation of "Curie" and "anti-Curie" behavior within the same molecule, *J. Phys. Chem. 99*, 17795−17804.
25. Banci, L., Bertini, I., Luchinat, C., Pierattelli, R., Shokhirev, N. V., and Walker, F. A. (1998) Analysis of the temperature dependence of the ^{1}H and ^{13}C isotropic shifts of horse heart ferricytochrome *c*: Explanation of Curie, anti-Curie and nonlinear pseudocontact shifts in a common two-level framework, *J. Am. Chem. Soc. 120*, 8472−8479.
26. Shokhirev, N. V., and Walker, F. A. (1995) Analysis of the temperature dependence of the ^{1}H contact shifts in low-spin Fe(III) model hemes and heme proteins: Explanation of "Curie" and "Anti-Curie" behavior within the same molecule, *J. Phys. Chem. 99*, 17795−17804.
27. Timkovich, R., and Cai, M. (1993) Investigation of the structure of oxidized *Pseudomonas aeruginosa* cytochrome *c*-551 by NMR: comparison of observed paramagnetic shifts and calculated pseudocontact shifts, *Biochemistry 32*, 11516−11523.
28. Kitahara, R., Sareth, S., Yamada, H., Ohmae, E., Gekko, K., and Akasaka, K. (2000) High pressure NMR reveals active-site hinge motion of folate-bound *Escherichia coli* dihydrofolate reductase, *Biochemistry 39*, 12789−12795.
29. Kitahara, R., Yamada, H., and Akasaka, K. (2001) Two folded conformers of ubiquitin revealed by high-pressure NMR, *Biochemistry 40*, 13556−13563.
30. Kitahara, R., Yamada, H., Akasaka, K., and Wright, P. E. (2002) High Pressure NMR reveals that apomyoglobin is an equilibrium mixture from the native to the unfolded, *J. Mol. Biol. 320*, 311−319.
31. Kitahara, R., and Akasaka, K. (2003) Close identity of a pressure-stabilized intermediate with a kinetic intermediate in protein folding, *Proc. Natl. Acad. Sci. U.S.A. 100*, 3167−3172.
32. Hata, K., Kono, R., Fujisawa, M., Kitahara, R., Kamatari, Y. O., Akasaka, K., and Xu, Y. (2004) High pressure NMR study of dihydrofolate reductase from a deep-sea bacterium *Moritella profunda*, *Cell. Mol. Biol. 50*, 311−316.
33. Kitahara, R., Yokoyama, S., and Akasaka, K. (2005) NMR snapshots of a fluctuating protein structure: ubiquitin at 30 bar-3 kbar, *J. Mol. Biol. 347*, 277−285.
34. Kitahara, R., Okuno, A., Kato, M., Taniguchi, Y., Yokoyama, S., and Akasaka, K. (2006) Cold denaturation of ubiquitin at high pressure, *Magn. Reson. Chem. 44*, 108−113.
35. La Mar, G. N., Satterlee, J. D., and de Ropp, J. S. (2000) Nuclear magnetic resonance of hemoproteins, in *The Porphyrin Handbook* (Kadish, K., Smith, K. M., and Guilard, R., Eds.) pp 185−298, Academic Press, New York.
36. Bertini, I., and Luchinat, C. (1986) *NMR of Paramagnetic Molecules in Biological Systems*, pp 19−46, The Benjamin/Cummings, Menlo Park, CA.
37. Yamamoto, Y. (1998) NMR study of active sites in paramagnetic hemoproteins, *Annu. Rep. NMR Spectrosc. 36*, 1−77.
38. Barker, P. D., and Ferguson, S. J. (1999) Still a puzzle: why is haem covalently attached in *c*-type cytochromes?, *Structure 7*, R281−R290.
39. Shokhirev, N. V., and Walker, F. A. (1998) The effect of axial ligand plane orientation on the contact and pseudocontact shifts of low-spin ferriheme proteins, *J. Biol. Inorg. Chem. 3*, 581−594.
40. Shokhirev, N. V., and Walker, F. A. (1998) Co- and counterrotation of magnetic axes and axial ligands in low-spin ferriheme systems, *J. Am. Chem. Soc. 120*, 981−990.
41. Walker, F. A. (1999) in *The Porphyrin Handbook* (Kadish, K. M., Smith, K. M., and Guillard, R., Eds.) pp 81−183, Academic Press, San Diego, CA.
42. Bertini, I., Luchinat, C., Parigi, G., and Walker, F. A. (1999) Heme methyl ^{1}H chemical shifts as structural parameters in some low spin ferriheme proteins, *J. Biol. Inorg. Chem. 4*, 515−519.
43. Banci, L., Bertini, I., Cavallaro, G., and Luchinat, C. (2002) Chemical shift-based constraints for solution structure determination of paramagnetic low-spin heme proteins with bis-His and His-CN^{-} axial ligands: the cases of oxidized cytochrome b_5 and Met80Ala cyano-cytochrome *c*, *J. Biol. Inorg. Chem. 7*, 416−426.
44. Turner, D. L. (1995) Determination of haem electronic structure in His-Met cytochromes *c* by ^{13}C-NMR. The effect of the axial ligands, *Eur. J. Biochem. 227*, 829−837.
45. Tachiiri, N., Hemmi, H., Takayama, S. J., Mita, H., Hasegawa, J., Sambongi, Y., and Yamamoto, Y. (2004) Effects of axial methionine coordination on the in-plane asymmetry of the heme electronic structure of cytochrome *c*, *J. Biol. Inorg. Chem. 9*, 733−742.
46. Misumi, Y., Terui, N., and Yamamoto, Y. (2002) Structural characterization of non-native states of sperm whale myoglobin in aqueous ethanol of 2,2,2-trifluoroethanol media, *Biochim. Biophys. Acta 1601*, 75−84.
47. Timkovich, R., Bergmann, D., Arciero, D. M., and Hooper, A. B. (1998) Primary sequence and solution conformation of ferrocytochrome *c*-552 from *Nitrosomonas europaea*, *Biophys. J. 75*, 1964−1972.
48. Chen, Y., Liang, Q., Arciero, D. M., Hooper, A. B., and Timkovich, R. (2007) Heme crevice disorder after sixth ligand displacement in the cytochrome *c*-551 family, *Arch. Biochem. Biophys. 457*, 95−104.
49. Terui, N., Tachiiri, N., Matsuo, H., Hasegawa, J., Uchiyama, S., Kobayashi, Y., Igarashi, Y., Sambongi, Y., and Yamamoto, Y. (2003) Relationship between redox function and protein stability of cytochromes *c*, *J. Am. Chem. Soc. 125*, 13650−13651.
50. Takayama, S. J., Mikami, S., Terui, N., Mita, H., Hasegawa, J., Sambongi, Y., and Yamamoto, Y. (2005) Control of the redox potential of *Pseudomonas aeruginosa* cytochrome c_{551} through

the Fe-Met coordination bond strength and pK_a of a buried heme propionic acid side chain, *Biochemistry 44*, 5488−5494.

51. Cohen, D. S., and Pielak, G. J. (1995) Entropic stabilization of cytochrome *c* upon reduction, *J. Am. Chem. Soc. 117*, 1675−1677.
52. Christen, R. P., Nomikos, S. I., and Smith, E. T. (1996) Probing protein electrostatic interactions through temperature/reduction potential profiles, *J. Biol. Inorg. Chem. 1*, 515−522.
53. Li, C., Yanagisawa, S., Martins, B. M., Messerschmidt, A., Banfield, M. J., and Dennison, C. (2006) Basic requirements for a metal-binding site in a protein: The influence of loop shortening on the cupredoxin azurin, *Proc. Natl. Acad. Sci. U.S.A. 103*, 7258−7263.
54. Li, C., Benfield, M. J., and Dennison, C. (2007) Engineering copper sites in proteins: Loop confer native structures and properties to chimeric cupredoxins, *J. Am. Chem. Soc. 129*, 709−718.
55. Karan, E. F., Russell, B. S, and Bren, K. L. (2002) Characterization of *Hydrogenobacter thermophilus* cytochromes c_{552} expressed in the cytoplasm and periplasm of *Escherichia coli*, *J. Biol. Inorg. Chem. 7*, 260−272.

BI7000714